



OPEN

Electrodeposition and analysis of thick bismuth films

Kendrich O. Hatfield¹, Enkeleda Dervishi^{1✉}, Don Johnson¹, Courtney Clark¹, Nathan Brown¹, Genevieve C. Kidman¹, Darrick J. Williams² & Daniel E. Hooks^{1,2}

Due to its unique physical and chemical properties, bismuth is an attractive candidate for a wide range of applications such as battery anodes, radiation shielding, and semiconductors, to name a few. This work presents the electrodeposition of mechanically stable and homogenous bismuth films at micron-scale thicknesses. A simple one-step electrodeposition process using either a pulse/reverse or direct current source yielded thick, homogenous, and mechanically stable bismuth films. Morphology, electrochemical behavior, adhesion, and mechanical stability of bismuth coatings plated with varying parameters were characterized via optical profilometry, cyclic voltammetry, electron microscopy, and tribology. Scratch testing on thick electroplated coatings (> 100 μm) revealed similar wear resistance properties between the pulse/reverse plated and direct current electroplated films. This study presents a versatile bismuth electroplating process with the possibility to replace lead in radiation shields with an inexpensive, non-toxic metal, or to make industrially relevant electrocatalytic devices.

Bismuth is a semimetal with interesting physical, electrical, and chemical properties^{1,2}. Its unique properties, low toxicity³, and availability lead to many applications, such as battery anodes⁴, semiconductors for electrocatalytic degradation of organic waste⁵, and superconductors⁶. Moreover, Bi has a high hydrogen evolution overpotential, allowing higher current efficiency for reductive processes in electrochemical devices, and it has a high electrocatalytic activity toward CO₂ reduction⁷. Bi is also an effective radiation shielding material^{8,9} and has high magnetoresistance¹⁰, making it useful in a variety of other applications such as radiation safety and magnetic sensing. Several methods such as sputtering¹¹, thermal evaporation¹², molecular beam epitaxy¹³, and electrodeposition^{1,2,14} have been used to fabricate Bi films. Electrodeposition is particularly attractive, being amenable to mild temperature and pressure conditions on irregularly shaped substrates of a wide range of sizes, with great control over resulting surface morphology¹⁰. Previous studies have demonstrated electrodeposition of Bi, generally obtaining nanometer¹⁴ to single micron^{1,15} thicknesses. For some practical applications (particularly radiation shielding), thicker, robust films are desirable¹⁶. Millimeter-scale electrodeposited Bi coatings have been previously demonstrated a few times in literature on copper films¹⁶ and a nickel-phosphorous coating¹⁷ using constant current density deposition methods. However, pulsed electrodeposition is regularly employed to improve coating deposition and brightness¹⁸, and has been used before for thinner Bi coatings¹⁹. Possible benefits include a more dense and uniform coating due to the steeper concentration gradient at the surface, as well as better control over film morphology. This work demonstrates a simple, one-step process for depositing Bi films > 100 μm thick with subsequent examination of the effects of pulsed vs direct current plating, differing current densities, and deposition time. Coatings were characterized via electron microscopy, cyclic voltammetry, and tribology to fully understand their structure, adhesion, and mechanical stability.

Materials and Electrodeposition

Electrodeposition. Potassium hydroxide (VWR, reagent grade), tartaric acid (Acros organics, 99+%), bismuth (III) nitrate pentahydrate (either Alfa Aesar, 98% or Acros organics, 99.999%), glycerol (VWR, biotechnology grade), and nitric acid (Millipore-Sigma, Emplura, 65%) were used as received for electrodeposition. The plating solution consisted of bismuth nitrate (0.15 M), glycerol (1.4 M), KOH (1.2 M), tartaric acid (0.33 M), and HNO₃ to adjust pH, which was measured with a Thermo Scientific Orion Star A221 pH meter equipped with a Thermo Scientific 9107BNMD triode. A Dynatronix DuPR10-3-6XR power supply was used with a two-electrode configuration: platinized titanium as an anode/counter electrode (CE) and a gold-plated brass or steel panel (5 μm thick) as the cathode/working electrode. The electrodes were suspended in a glass beaker filled with the plating solution with a magnetic stir bar over a stir plate for all electrodeposition processes. All experiments were performed at room temperature.

¹SIGMA-2: Finishing Manufacturing Science, Los Alamos National Laboratories, SM-30 Bikini Atoll Road, Los Alamos, NM 87545, USA. ²MPA-CINT: Center for Integrated Nanotechnologies, Los Alamos National Laboratories, Los Alamos, NM 87544, USA. ✉email: enkeleda@lanl.gov

Bismuth film analysis. An Apreo 1 or 2 SEM with an EDAX or Oxford EDS attachment was used for SEM characterization including electron backscatter diffraction (EBSD). Apex OIM software was used to analyze EBSD data. Accelerating voltage for all SEM images was 20 kV. An SP-300 Biologic potentiostat was used with a 3-electrode configuration with a standard calomel reference electrode (saturated KCl), a carbon rod CE, and electrodeposited bismuth working electrode to test hydrogen evolution reaction (HER) on electroplated bismuth in 10% HNO₃. An RTEC MFT-5000 tribometer was used with a Rockwell type C tip for progressive load scratch testing from 0.1 to 40 N. Prior to tribological tests, Bi films were polished with 10–12 μm (800 grit) sandpaper. A Keyence VK-1000X optical profilometer was used to image films for roughness and assess wear volumes for tribological scratch tests.

XRD was performed on a Rigaku Ultima III diffractometer with fine line sealed Cu tube Kα ($\lambda = 1.5406 \text{ \AA}$) x-rays and a D/MAX Ultima series with a maximum power of 3 kW. XRD data was collected on a continuous scan mode in Bragg–Brentano slit geometry over a 2-theta range of 5°–90° with sampling width of 0.05° and scanning speed of 1.5°/min. The divergence slit was set to 2.0 mm, the divergence H.L. slit was set at 10 mm, and the scattering and receiving slits were set to open and open.

Results and discussion

Understanding the effects of electrodeposition parameters. Many parameters profoundly affect Bi electroplating, making proper conditions paramount to obtaining a film with homogenous surface coverage and good adhesion. In addition to Bi(NO₃)₃, we added tartaric acid and glycerol as chelating agents in the same manner as Chen et al.¹⁵ to help moderate film growth¹⁰ and stabilize Bi³⁺ ion. Plating in this solution is highly sensitive to solution pH, with the best coating obtained at a pH range of 0.01–0.1, resulting in a robust film, while higher pH values produce a film with poor adhesion, able to be wiped away easily by hand. For all further experiments, we adjusted the pH to ~0.08 with HNO₃ before plating. Current density was found to significantly affect film quality; samples plated with current densities of 180 mA/cm² and 50 mA/cm² had inconsistent topographies, with Sa values generally greater than 50 μm and poor adhesion, often delaminating from the substrate upon removal from the electrolyte. Thus, we used a current density of 1.5 mA/cm² for later experiments. Figure 1 shows optical profilometry and photos of intact films grown with direct currents of 50 mA/cm² for 17 h, 2.5 mA/cm² for 24 h, and 1.5 mA/cm² for 24 h. Sandnes et al. reported that current densities above 10 mA/cm² resulted in significantly rougher films¹, agreeing with our results. Current densities of 1.5 mA/cm² (Sa of 5.2 μm) and 2.5 mA/cm² (Sa of 2.6 μm) yielded the brightest and smoothest films.

Pulsed and direct current electrodeposited bismuth. Many researchers have used pulsed electro-deposition with a variety of pulse waveforms to obtain more uniform films, higher plating efficiency, and control

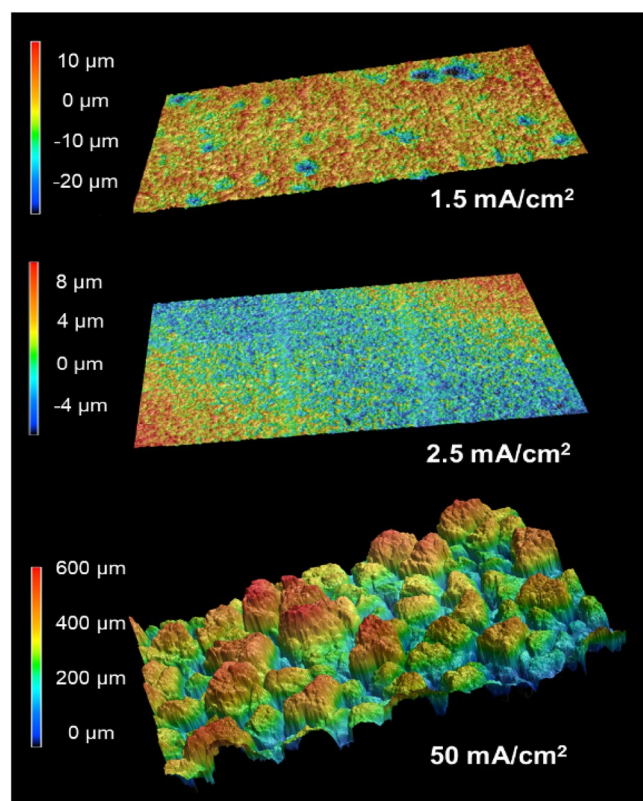


Figure 1. Optical profilometry of intact Bi films electrodeposited at 50 mA/cm², 2.5 mA/cm², and 1.5 mA/cm².

over morphologies and grain sizes²⁰. Pulses used range from sub-millisecond to second timescales and can include “reverse” pulses (i.e. a stripping current) which can improve film uniformity²⁰. While a full study of different pulse sequences is beyond the scope of this article, we tested Bi electrodeposition using a pulse/reverse plating process with millisecond-scale pulses (waveform shown in Fig. 2) and compared the resulting coatings with those obtained with direct current plating.

We used a current density of 1.5 mA/cm^2 for both pulsed and DC depositions and plated samples for 24 and 96 h. Figure 3 shows SEM images of each sample. The DC-plated samples both show elongated features on the surface, with those on the 96-h DC sample being very thin. On the other hand, the pulse-plated samples displayed a mixed morphology with regions of both elongated features like the 24-h DC sample and “blockier” morphologies with features roughly $2\text{--}5 \mu\text{m}$ in diameter, similar to those found by Gades, et al.²¹. This implies that the electrodeposition waveform has an effect on surface morphology which in turn has been shown to affect electrocatalytic properties¹⁹. We also observed grains with EBSD on polished cross-sections of 96-h plated samples and estimated grain sizes of $19 \mu\text{m}$ for the DC-plated coating and $41 \mu\text{m}$ for the pulse-plated coating (Fig. 4, size histogram in Figure S1). Generally, pulse-plating leads to finer grains than direct current²², but our results for the DC-plated grains are likely skewed by the high presence of suspected twinning. Overall, our results indicate that this electrodeposition method offers control over film microstructure, which can significantly impact the physical properties of metals²³.

We measured film thicknesses (summarized along with deposition rate and deposition efficiency in Table 1) by cross-sectional SEM (Figure S2); thicknesses varied widely for the 24-h pulse/reverse and DC-plated samples, from 80 to $290 \mu\text{m}$. As others have previously noted, film thickness is heavily affected by hydrodynamics (i.e.

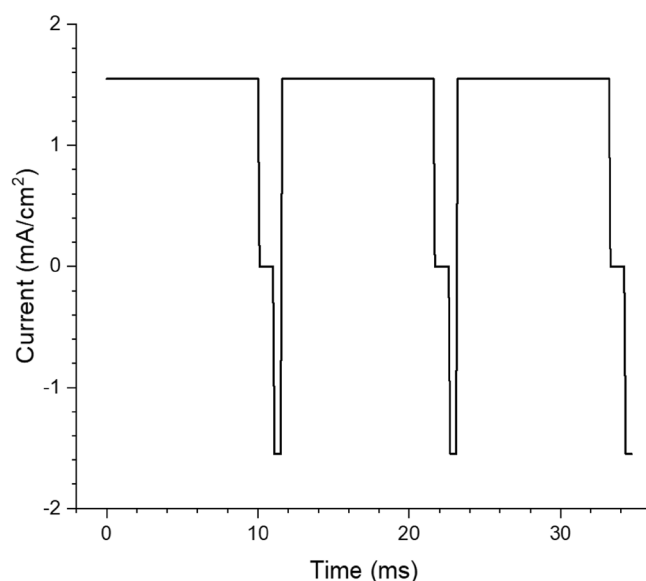


Figure 2. Waveform of the current-controlled pulsed plating process. Both the reverse and forward pulses were 1.5 mA/cm^2 .

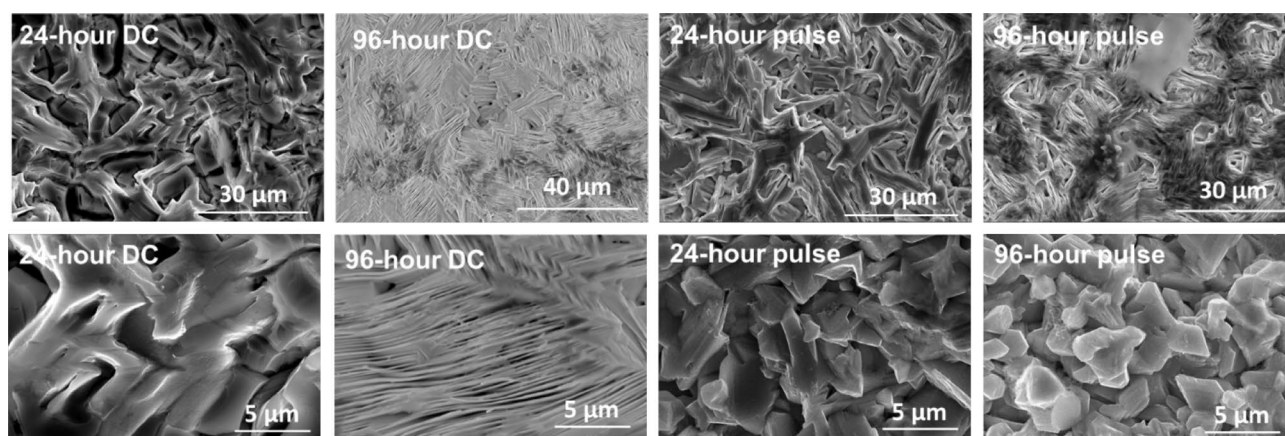


Figure 3. Scanning electron microscopy (20 kV accelerating voltage) of electroplated bismuth at various magnifications.

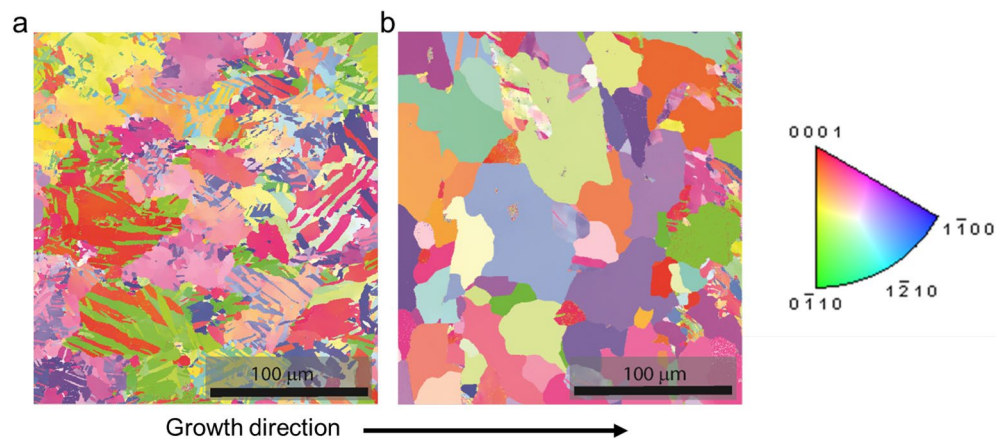


Figure 4. EBSD of 96-h (a) DC-plated and (b) pulse-plated bismuth coatings.

Deposition parameters	Coating thickness (μm)	Deposition rate ($\mu\text{m}/\text{h}$)	Deposition efficiency (%)
24-h DC	80–290	3.3–12	98
96-h DC	330–500	3.6–5.1	72
24-h pulse	90–260	4.0–10.6	91
96-h pulse	230–320	2.5–3.1	83

Table 1. Electrodeposition results.

stirring/bath geometry) and cathode placement^{24,25}, though the majority of our films were $\geq 100 \mu\text{m}$. The 96-h electroplated samples had more consistent thicknesses with DC-plating yielding thicker films than pulsed-plating, likely due to the lower effective current (i.e. duty cycle) of the pulse sequence. These results indicate that either pulsed or DC electroplating is effective to obtain thick ($> 100 \mu\text{m}$) Bi films with good coverage at high deposition efficiencies ($> 70\%$).

An EDS linescan of a Bi-plated cross-section (96-h pulse-plated) shows clear separation between the bismuth, gold, and steel layers on the panel (Fig. 5a). Figure 5b shows overlaid individual EDS spectra of these regions. All samples showed comparable EDS results, shown in Figure S3, and Figure S4 shows an EDS map evidencing a homogenous Bi coverage on the sample surface.

We also performed XRD on a polished Bi surface (24-h pulse-plated) that matches that for Bi (Fig. 6)^{26,27}.

Electrochemical testing. To test the HER activity of electroplated Bi, a critical parameter in electrocatalytic applications, we performed cyclic voltammetry at 20 mV/s on 24-h pulse- and DC-plated bismuth films and plain gold in 10% HNO_3 . Figure 7 shows the higher overpotential of HER on Bi vs Au in the overlaid voltammograms. This is in agreement with Sandnes, et al.¹, and indicates sufficient coverage of Bi to isolate gold from the

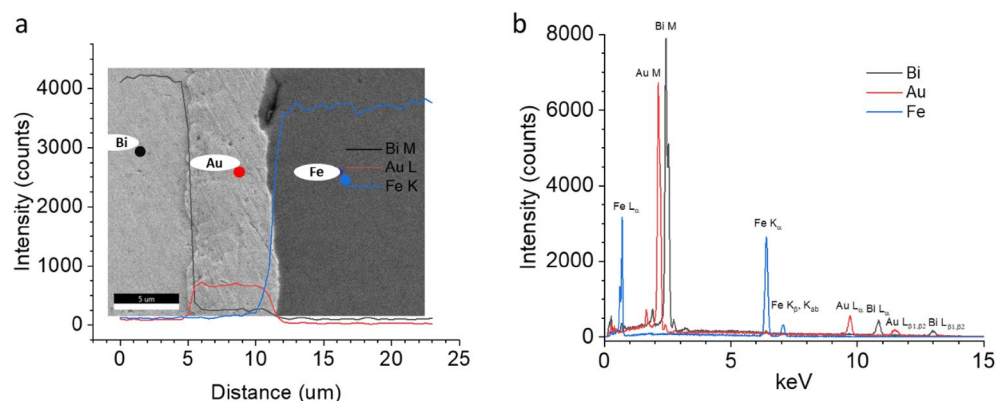


Figure 5. EDS of a bismuth-plated sample cross-section. (a) Linescan data across the cross-section from the bismuth M line (black), gold L line (red), and iron K line (blue). (b) Overlaid EDS spectra of bismuth (black), gold (red), and iron (blue) areas in the cross section.

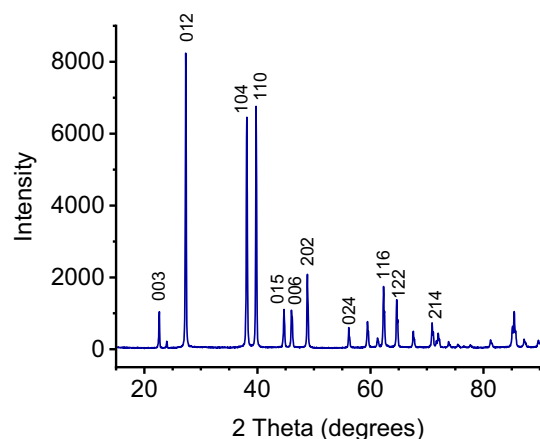


Figure 6. XRD of a polished 24-h pulse-plated Bi coating.

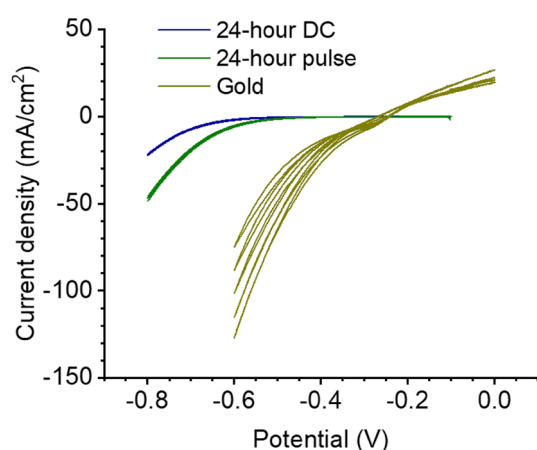


Figure 7. Hydrogen evolution reaction on 24-h pulse- and DC-plated bismuth compared to gold. Cyclic voltammetry performed at 20 mV/s in 10% HNO_3 using a standard calomel reference electrode (saturated KCL) and a carbon rod counter electrode.

solution. The pulse-plated sample yielded lower overpotentials for HER as compared to the DC sample, implying a difference in electrocatalytic activity between the two. This shows promise for electrochemical tunability based on electrodeposition parameters.

Mechanical properties. Mechanically robust films are required for practical applications of these films such as radiation shields. We used progressive load scratch testing from 0.1 to 40 N to evaluate tribological performance via the critical load of failure characterized by delamination of the coating from the substrate in the form of gross spallation (Fig. 8—at least 3 scratch tests per sample)²⁸. On the thinner 24-h plated samples ($\sim 100 \mu\text{m}$), the scratch stylus broke through the Bi at 25 N for both pulse and DC-plated samples, exposing gold, but without substantial delaminating or cracking of the surrounding bismuth film. Figure 8 demonstrates the EDS maps of the scratch test area for the pulse-plated Bi films at various times. The thicker samples ($< 200 \mu\text{m}$) withstood up to 40 N (the force limit on our scratch measurement setup) without breaking through to the gold. The wear volume of the scratches, as measured by an optical profilometer, on the 96-h DC plated film were $0.029 \pm 0.011 \text{ mm}^3$, while the wear volume for the 96-h pulse plated sample were $0.035 \pm 0.011 \text{ mm}^3$, indicating similar resistance to scratching between the two plating methods. These results are evidence for good adhesion of the Bi to the Au and robustness for radiation shielding applications regardless of pulse waveform.

Conclusions

In this study, we demonstrated a simple, non-toxic process for electrodepositing thick ($> 100 \mu\text{m}$) Bi films on gold substrates and evaluated the effects of deposition time and pulsed vs DC electroplating. Increasing deposition times with both constant current and pulse/reverse methods lead to thicker films, showing potential for industrially usable, robust films for radioactive shielding applications. EDS showed a relatively pure and homogenous distribution of Bi throughout the film regardless of deposition parameters with a current density of 1.5 mA/cm^2 .

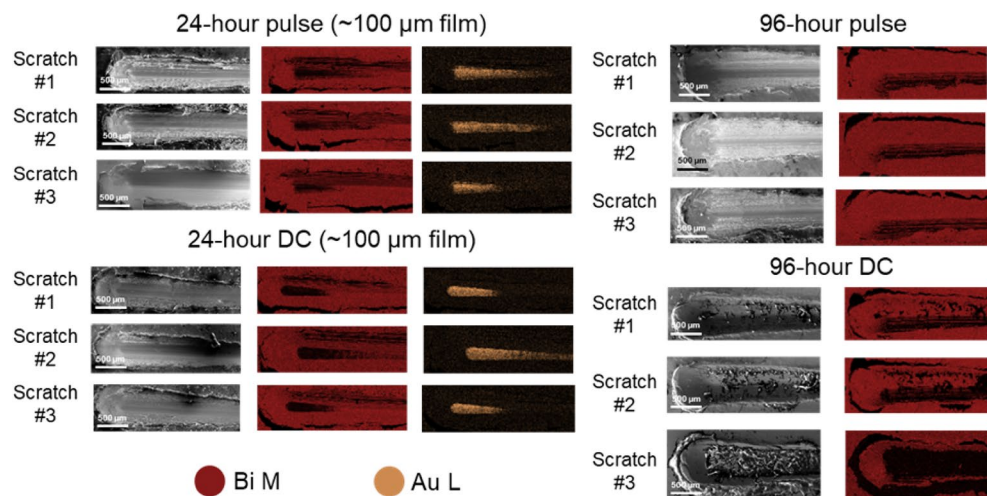


Figure 8. EDS maps of pulse-plated Bi films showing film breakthrough on $\sim 100\ \mu\text{m}$ 24-h samples, but not 96-h samples. Maps were made using Bi M lines and Au M lines.

Pulsed electrodeposition impacts surface morphology, grain size, and electrocatalytic activity of the electrolyte. Cyclic voltammetry showed higher HER activity on a pulse-plated sample compared to a DC-plated coating, implying a tunability for practical electrochemical applications. Mechanical strengths of DC- and pulse-plated coatings were similar, with scratch testing showing complete breakthrough of thin 24-h plated samples at 25 N with a Rockwell tip without excessive cracking or delamination. Scratch testing on samples $> 200\ \mu\text{m}$ also revealed similar wear resistance properties between DC and pulse plated films. Due to the versatility of electroplating toward substrates of irregular shapes and sizes, this study demonstrates a practical method of replacing lead in radiation shields with an inexpensive, non-toxic metal or for making industrially relevant electrocatalytic devices. Future experiments could involve testing films of varying thicknesses in a radioactive shielding environment or for carbon dioxide reduction to evaluate optimal Bi coating parameters for these applications.

Data availability

All data generated or analyses during this study are included in this published article [and its supplementary information files].

Received: 9 November 2022; Accepted: 11 January 2023

Published online: 21 January 2023

References

- Sandnes, E., Williams, M. E., Bertocci, U., Vaudin, M. D. & Stafford, G. R. Electrodeposition of bismuth from nitric acid electrolyte. *Electrochim. Acta* **52**, 6221–6228 (2007).
- Yang, M. & Hu, Z. Electrodeposition of bismuth onto glassy carbon electrodes from nitrate solutions. *J. Electroanal. Chem.* **583**, 46–55 (2005).
- Keogan, D. M. & Griffith, D. M. Current and potential applications of bismuth-based drugs. *Molecules* **19**, 15258–15297 (2014).
- Zhang, R., Bao, J., Wang, Y. & Sun, C. Concentrated electrolytes stabilize bismuth-potassium batteries. *Chem. Sci.* **9**, 6193–6198 (2018).
- Meng, X. & Zhang, Z. Bismuth-based photocatalytic semiconductors: Introduction, challenges and possible approaches. *J. Mol. Cat. A Chem.* **423**, 533–549 (2016).
- Sato, K. *et al.* Bismuth superconducting wires and their applications. *Cryogenics* **33**(3), 243–246 (1993).
- Abdallah, R. *et al.* New porous bismuth electrode material with high surface area. *J. Electroanal. Chem.* **839**, 32–38 (2019).
- Elsafi, M., El-Nahal, M. A., Sayyed, M. I. & Abbas, M. I. Novel 3-D printed radiation shielding materials embedded with bulk and nanoparticles of bismuth. *Sci. Rep.* **12**, 12467 (2022).
- Wang, B., Ting, C., Lai, C. & Tsai, Y. Bismuth pelvic X-ray shielding reduced radiation dose exposure in pediatric radiography. *Biomed. Res. Int.* **2021**, 9985714 (2021).
- Jiang, S., Huang, Y., Luo, F., Du, N. & Yan, C. Synthesis of bismuth with various morphologies by electrodeposition. *Inorg. Chem. Commun.* **6**, 781–785 (2003).
- Stanley, S. A. & Cropper, M. D. Structure and resistivity of bismuth thin films deposited by pulsed DC sputtering. *Appl. Phys. A* **120**, 1461–1468 (2015).
- Kumari, L. *et al.* Effects of deposition temperature and thickness on the structural properties of thermal evaporated bismuth thin films. *Appl. Surf. Sci.* **253**, 5931–5938 (2007).
- Chen, T. *et al.* Stabilizing lithium metal anode by molecular beam epitaxy grown uniform and ultrathin bismuth film. *Nano Energy* **76**, 105068 (2020).
- Prados, A. & Ranchal, R. Electrodeposition of Bi films on H covered n-GaAs(111)B substrates. *Electrochim. Acta* **305**, 212–222 (2019).
- Chen, J. *et al.* Electroplating deposition of bismuth absorbers for X-ray superconducting transition edge sensors. *Materials* **14**, 7169 (2021).
- Tishkevich, D. I. *et al.* Functional Bi coatings as a perspective material for radiation shields production against electron radiation. *Adv. Mater. Lett.* **11**(2), 20021479 (2020).

17. Cybul'skaja, L. S.; Poznjak, S. K.; Perevoznikov, S. S.; Shendjukov, V. S.; Gaevskaja, T. V.; Grabchikov, S. S.; Tishkevich, D. I. Method for applying a thick-layer bismuth coating to aluminium and alloys thereof for manufacture of radiation screens. 2017.
18. Paunovic, M. Electrochemical aspects. In *Modern Electroplating, Electrochemical Society Series* 4th edn (eds Schlesinger, M. & Paunovic, M.) (Wiley, 2000).
19. Park, J. Y. *et al.* The effect of pulse electrodeposition of bismuth on electrochemical reduction of carbon dioxide to formate. *Electron. Mat. Lett.* **15**, 454–461 (2019).
20. Devaraj, G., Guruviah, S. & Seshadri, S. K. Pulse plating. *Mater. Chem. Phys.* **25**, 439–461 (1990).
21. Gades, L. M. *et al.* Development of thick electroplated bismuth absorbers for large collection area hard X-ray transition edge sensors. *IEEE Trans. Appl. Supercond.* **27**(4), 2101105 (2017).
22. Karimi, S. & Foulkes, F. R. Modeling the effects of different pulse current waveforms on grain size of electrodeposited nickel coatings. *J. Electrochem. Soc.* **159**(11), D659–D670 (2012).
23. Armstrong, R. W. The influence of polycrystal grain size on several mechanical properties of materials. *Metall. Mater. Trans. B* **1**, 1169–1176 (1970).
24. Tan, Y. & Lim, K. Y. Understanding and improving the uniformity of electrodeposition. *Surf. Coat. Technol.* **167**, 255–262 (2003).
25. Yang, G., Deng, D., Zhang, Y., Zhu, Q. & Cai, J. Numerical optimization of electrodeposition thickness uniformity with respect to the layout of anode and cathode. *Electrocatalysis* **12**, 478–488 (2021).
26. Lafuente, B., Downs, R. T., Yang, H. & Stone, N. The power of databases: The RRUFF project. In *Highlights in Mineralogical Crystallography* (eds Armbruster, T. & Danisi, R. M.) 1–30 (De Gruyter, 2015).
27. Sathiyaraj, P. & Samuel, E. J. Application of bi-nanoparticle on dose enhancement effect in two different polymer gel dosimeter using spectrophotometer. *J. Can. Res. Ther.* **14**(3), 662–665 (2018).
28. ASTM International. *Standard Test Method for Adhesion Strength and Mechanical Failure Modes of Ceramic Coatings by Quantitative Single Point Scratch Testing*; ASTM C1624–05 (2010).

Acknowledgements

The authors acknowledge the Laboratory Directed Research and Development (LDRD) funding programs at the Los Alamos National Laboratory for partially funding this work. This work was performed, in part, at the Center for Integrated Nanotechnologies, an Office of Science User Facility operated for the U.S. Department of Energy (DOE) Office of Science.

Author contributions

K.H.: Writing—original draft, Methodology, Formal analysis, Writing—review and editing. E.D.: Conceptualization, Investigation, Methodology, Formal analysis, Writing—review and editing. D.J.: Carried out the experiments, Investigation, Methodology. C.C.: Material Characterization and preparation. N.B.: Material Characterization and preparation. G.K.: Grain size characterization and discussion of results. D.W.: XRD characterization and discussion. D.E.H.: Conceptualization, Methodology, Writing—review and editing.

Competing interests

The authors declare no competing interests.

Additional information

Supplementary Information The online version contains supplementary material available at <https://doi.org/10.1038/s41598-023-28042-z>.

Correspondence and requests for materials should be addressed to E.D.

Reprints and permissions information is available at www.nature.com/reprints.

Publisher's note Springer Nature remains neutral with regard to jurisdictional claims in published maps and institutional affiliations.



Open Access This article is licensed under a Creative Commons Attribution 4.0 International License, which permits use, sharing, adaptation, distribution and reproduction in any medium or format, as long as you give appropriate credit to the original author(s) and the source, provide a link to the Creative Commons licence, and indicate if changes were made. The images or other third party material in this article are included in the article's Creative Commons licence, unless indicated otherwise in a credit line to the material. If material is not included in the article's Creative Commons licence and your intended use is not permitted by statutory regulation or exceeds the permitted use, you will need to obtain permission directly from the copyright holder. To view a copy of this licence, visit <http://creativecommons.org/licenses/by/4.0/>.

© The Author(s) 2023